J. Fluid Mech. (1995), *vol.* 291, *pp.* 139–161

Chaotic transport by dipolar vortices on a β-plane

By O. U. VELASCO FUENTES†, G. J. F. VAN HEIJST AND B. E. CREMERS

Fluid Dynamics Laboratory, Eindhoven University of Technology, P.O. Box 513, 5600 MB Eindhoven, The Netherlands

(Received 24 March 1994 and in revised form 29 November 1994)

During the meandering motion of a dipolar vortex on a β-plane mass is exchanged both between the dipole and the ambient fluid and between the two dipole halves. The mass exchange (as well as the meandering motion) is caused by variations of the relative vorticity of the vortices due to conservation of potential vorticity. Previous studies have shown that a modulated point-vortex model captures the essential features in the dipole evolution. For this model we write the equations of motion of passive tracers in the form of a periodically perturbed integrable Hamiltonian system and subsequently study transport using a 'dynamical-systems theory' approach. The amount of mass exchanged between different regions of the flow is evaluated as a function of two parameters: the gradient of ambient vorticity, β, and the initial direction of propagation of the dipole, α_0. Mass exchange between the dipole and the surroundings increases with increasing both β and α_0. The exchange rate (amount of mass exchanged per unit time) increases with β and has a maximum for a particular value of α_0 ($\approx 0.62\pi$). Dipolar vortices in a rotating fluid (with a sloping bottom providing the 'topographic' β-effect) show, in addition to the relative vorticity variations, a second perturbation that leads to exchange of mass. The points where vorticity is extreme approach each other as the dipole moves to shallower parts of the fluid and separate as the couple moves to deeper parts. This mechanism is studied independently and it is shown to lead to a stronger exchange between the dipole halves and the ambient fluid but no exchange between the two dipole halves.

1. Introduction

The dynamics of two-dimensional vortices has been intensively studied in recent years. Much of this interest comes from the geophysical fluid dynamics and plasma physics communities. In geophysical flows the two-dimensionality is caused by the geometry of the domain (horizontal scales generally being much larger than vertical scales), rotation and stratification; in plasmas two-dimensionality may be established by the presence of a magnetic field. The richness of phenomena exhibited by two-dimensional flows is further increased by the presence of inhomogeneities in the media: gradients of ambient vorticity are present in geophysical flows, primarily due to the variation of the Coriolis parameter with latitude, but variations of the fluid depth can effectively result in a gradient of ambient vorticity. In plasmas equivalent effects are produced by density gradients.

One particular vortex that has received much attention is the dipolar vortex. This vortex has two remarkable properties: it possesses a separatrix and it has a non-zero linear momentum. This means that the dipole provides an efficient mechanism for the transport of mass and momentum over large distances compared to the vortex radius.

† Present affiliation: CICESE, A.P. 2732; Ensenada, B.C., México.

In particular, oceanic dipolar vortices might play an important role in the transport of scalar properties such as heat, salt, nutrients and other biochemical components. It has also been suggested (McWilliams 1980) that an atmospheric blocking is in fact a huge westward travelling dipole (WTD) that remains stationary due to the eastward atmospheric circulation. This stable disturbance may have a latitudinal scale of up to 45° and can exist for a couple of days to two weeks. Coherent vortices may also be responsible for anomalous transport in magnetically confined plasmas (Yabuki, Ueno & Kono 1993; Horton 1984).

Fundamental processes such as propagation and collision of dipolar vortices on a β-plane have been studied numerically and analytically in recent years (e.g. Makino, Kamimura & Taniuti 1981; Nycander & Isichenko 1990). Most studies are based on the equivalent barotropic vorticity equation (or Hasegawa–Mima equation, as it is called in the context of plasma physics) and all have shown the same properties of the modulated point-vortex model introduced by Kono & Yamagata (1977), namely, meandering of a single dipole around lines of equal ambient vorticity and soliton-like collision of aligned identical dipoles.

More recently the meandering motion of a single vortex dipole on a (topographic) β-plane has been verified experimentally (Kloosterziel, Carnevale & Philippe 1993; Velasco Fuentes & van Heijst 1994, hereafter called VFvH). Kloosterziel *et al.* observed, in both visualization experiments and numerical simulations, the detrainment and entrainment of fluid in the form of a tail in the wake and spiral structures in the interior of the dipole, respectively. VFvH observed the same features in the visualization experiments and measured the alternating asymmetries in the stream function, which is the primary mechanism for entrainment and detrainment. A second mechanism for transport, only present on the topographic β-plane, was also observed in both visualizations and flow measurements. As the dipole moves uphill the distance between the two halves increases, causing entrainment of fluid, whereas when it moves downhill the dipole halves approach each other, resulting in detrainment of fluid.

In this particular case transport of fluid is dominated by advection so that the relative motions of fluid parcels are all important. The study of these motions ('Lagrangian' view) can be pursued if the velocity field of the flow ('Eulerian' view) is known for all times. Using the point-vortex approach, and given a particular set of initial conditions, the positions and strengths of the point vortices are known for all times, and consequently so is the stream function. The motion of individual particles, which is far more complex than the motion of the couple itself, can thus be extensively analysed using recent developments in the theory of nonlinear dynamical systems (Rom-Kedar, Leonard & Wiggins 1990; Wiggins 1992). The stream function is also time periodic, and the problem can be reduced to the study of transport in a two-dimensional map (the Poincaré map). First we identify the structures in the flow that are responsible for transport between different flow regions: the hyperbolic fixed points of the Poincaré map (stagnation points in the unperturbed flow field) and the associated invariant curves or *manifolds* passing through these points. The many intersections of these manifolds form a complicated structure (*heteroclinic tangle*) that is responsible for the transport of fluid between different regions of fluid. Knowledge of the dynamics of the heteroclinic tangle enables us to calculate the amount of mass exchanged between the two dipole halves as well as between the dipole halves and the ambient fluid.

This 'dynamical-systems theory' approach was used by Rom-Kedar *et al.* (1990) to study chaotic particle motion due to a point-vortex dipole embedded in an oscillating external strain-rate field. Their work should be consulted by readers interested in a

more detailed discussion of the techniques used in the following sections. Hobson (1991*a*, *b*) used the point-vortex model to study the motion of dipolar vortices on the β-plane as well as the advection of passive tracers. It was shown that the stable and unstable manifolds intersect transversally and therefore that the motion of particles is chaotic (Hobson 1991*a*).

A dipolar vortex on the γ-plane (a plane where the Coriolis parameter changes quadratically with the distance to the pole) shows the same qualitative behaviour as the dipole on the β-plane, namely periodical meandering motion around lines of equal ambient vorticity (Yabuki *et al.* 1993; Velasco Fuentes 1994). Consequently, the exchange of mass between the dipolar vortex and the ambient fluid obeys the same mechanism as the one discussed here, with the difference that the dipolar vortex is confined to a certain region of the plane and periodically returns to regions where it has been before (Velasco Fuentes 1994).

The present paper is organized as follows: in §2 fluid exchange between the dipole and the ambient fluid is illustrated in an experiment and the physical mechanism for transport is discussed; in §3 the equations of motion of passive particles in the velocity field of a modulated point-vortex dipole are written in the form of a periodically perturbed integrable Hamiltonian system and a few important results on the theory of transport in dynamical systems are reviewed; in §4 the numerical results of transport in this model are presented; §5 is devoted to a perturbation specific to the 'topographic' β-plane, namely the variation of the distance between the dipole's halves as the vortex moves into shallower or deeper regions of the flow; in §6 we make a comparison between the point-vortex model and experimental observations for a few points in the parameter space. Finally we summarize and give some conclusions in §7.

2. The physical mechanism for transport

For the motion of an inviscid homogeneous fluid in a shallow layer on a planet rotating at a constant angular velocity Ω_E one may derive the following conservation relation:

$$\frac{\mathrm{D}}{\mathrm{D}t}\left(\frac{\omega+f}{h(x,y)}\right)=0, \tag{1}$$

where $\mathrm{D}/\mathrm{D}t \equiv \partial/\partial t + \boldsymbol{u}\cdot\boldsymbol{\nabla}$ is the material derivative in two dimensions; ω is the vertical component of the relative vorticity $\boldsymbol{\omega} \equiv \boldsymbol{\nabla}\times\boldsymbol{u} = (0,0,\omega)$; $f = 2\Omega_E \sin\phi$ is the Coriolis parameter, denoting the (local) vertical component of the ambient vorticity as a function of the latitude ϕ; and $h(x,y)$ is the fluid depth.

Let us first consider the case of a layer of fluid with constant depth h_0. The horizontal dimensions are assumed to be small, so that (i) the curvature of the domain enters (1) only through the variation of the Coriolis parameter; and (ii) the Coriolis parameter changes linearly in the north–south direction y, i.e. $f = f_0 + \beta y$, where $f_0 = 2\Omega_E \sin\phi_0$ and $\beta = (2\Omega_E/R)\cos\phi_0$, with R the Earth's radius. This approximation is known as the β-plane model and leads to a simplified expression for conservation of potential vorticity:

$$\frac{\mathrm{D}}{\mathrm{D}t}(\omega+\beta y)=0. \tag{2}$$

Let us assume now that the Coriolis parameter is constant in space, $f = f_0$, which is the case in a rotating (laboratory) tank and is a good approximation for motions in the ocean or in the atmosphere with a scale of about 100 km. Let h have a small linear variation in some direction, say y, so that the fluid depth as a function of position is

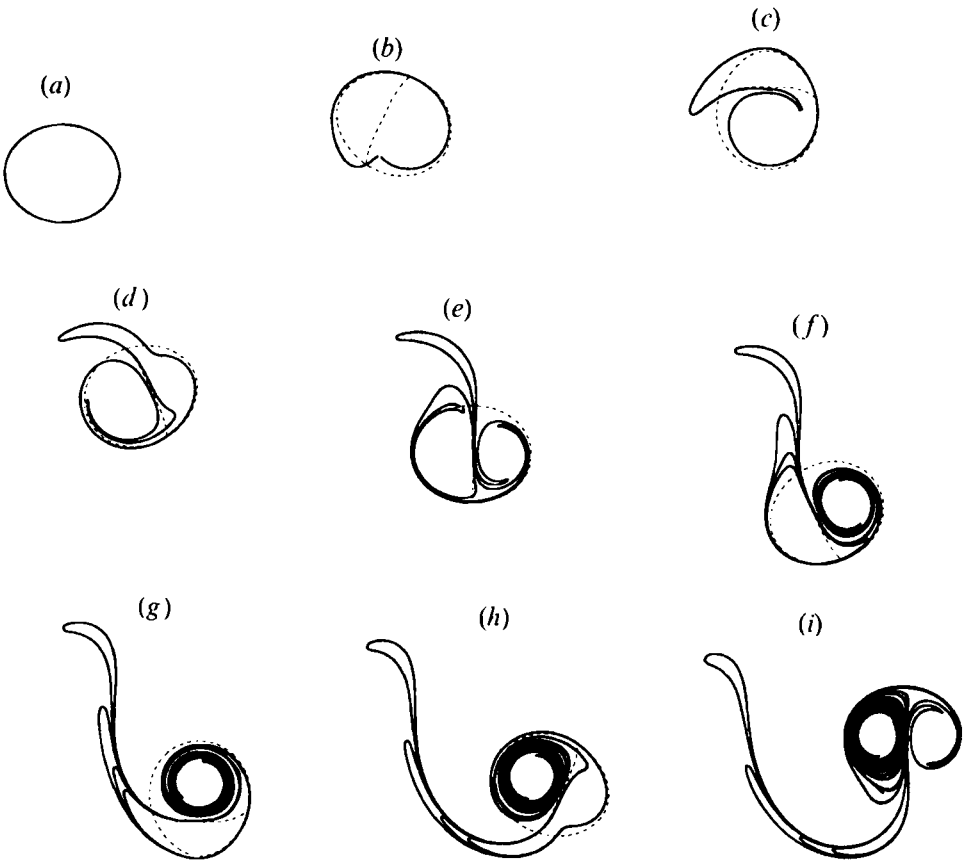

FIGURE 1. Evolution of a dipolar vortex on the β-plane according to the modulated point-vortex model. The thick line is the boundary of the fluid that initially lies within the unperturbed separatrix. The broken line represents the instantaneous separatrix. Time increases from left to right and from top to bottom and the interval between subsequent frames is approximately one eighth of the oscillation period.

given by $h(y) = h_0(1 - sy)$, with s a small parameter. Substituting this expression in (1) and expanding the result in a Taylor series one obtains

$$\frac{\mathrm{D}}{\mathrm{D}t}(\omega + sf_0 y) = 0, \tag{3}$$

where a small Rossby number ($\omega/f_0 \ll 1$) is assumed. This equation is equivalent to (2), showing that to this order of approximation the dynamics of a rotating fluid in a container with a linearly varying bottom topography is equivalent to that of a fluid on a β-plane, with the new 'gradient of ambient vorticity' given by $\beta = sf_0$.

The dynamical equivalence between the bottom topography and the gradient of the Coriolis parameter is used to study β-plane dipoles in the laboratory. Experiments were carried out in a rectangular tank of horizontal dimensions 100×150 cm^2 and 30 cm depth mounted on a table rotating with angular speed $\Omega_E = 0.56$ s^{-1}, so that the Coriolis parameter $f_0 = 2\Omega_E = 1.12$ s^{-1}. A false bottom was raised 4 cm along one of the long sides to provide the (topographic) β-effect and the fluid depth at the centre of the tank was chosen to be 13 cm and 23 cm. With these parameter settings the equivalent value of β measured 0.194 and 0.344 m^{-1} s^{-1}, respectively.

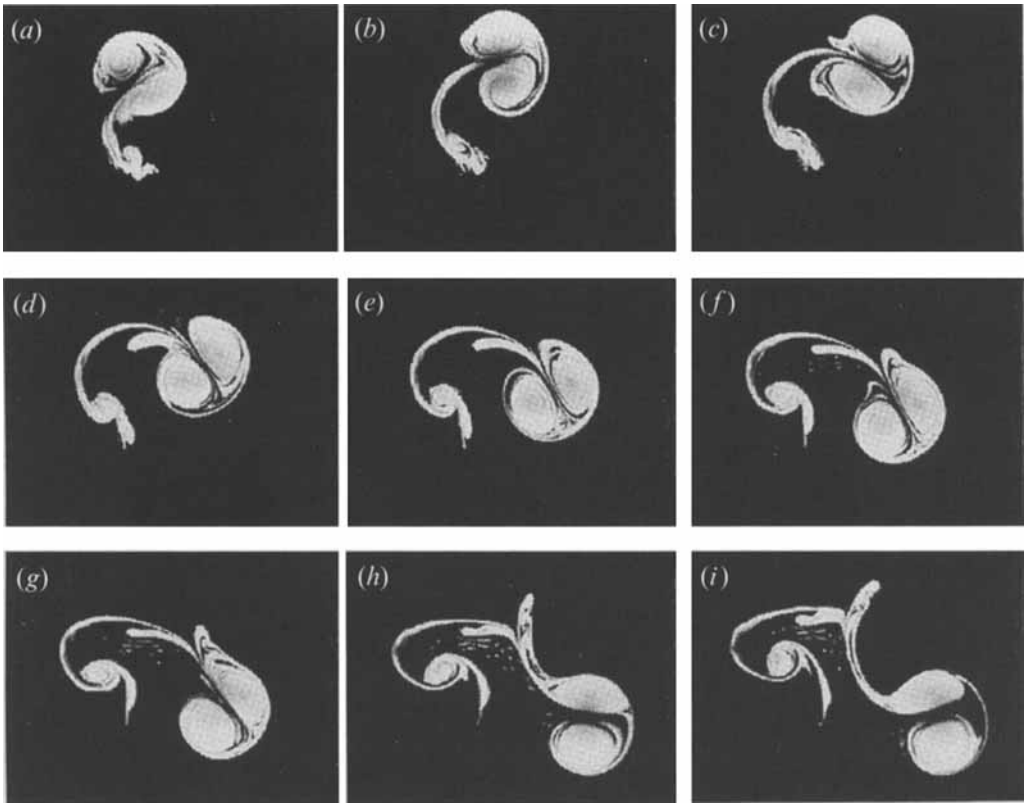

FIGURE 2. Sequence of experimental images showing the meandering of a dipolar vortex on a topographic β-plane. The dipole travelled initially northward (i.e. towards shallower fluid). The images were taken at times (*a*) $t = 30$ s, (*b*) 45 s, (*c*) 60 s, (*d*) 75 s, (*e*) 90 s, (*f*) 105 s, (*g*) 120 s, (*h*) 160 s, (*i*) 190 s, after withdrawing the cylinder. Experimental parameters: $f = 1.12\ \mathrm{s}^{-1}$, $h_0 = 0.13$ m, $s = 0.3\ \mathrm{m}^{-1}$, $\beta = 0.344\ \mathrm{m}^{-1}\ \mathrm{s}^{-1}$.

A two-dimensional dipole vortex was generated by slowly moving a small, bottomless cylinder of 8 cm diameter in a straight line relative to the rotating tank, while gradually lifting it. The vorticity generated by the motion of the cylinder accumulates in a dipolar structure in the wake of the cylinder. This dipolar flow is confined in a vertically aligned Taylor column, a feature well-known in rotating fluids. Dye (fluorescein) was added to the fluid within the small cylinder before the start of the experiment. In each experiment the flow was recorded with a video camera mounted in the rotating frame about 150 cm above the free surface of the fluid.

Let us recall the evolution of a modulated point-vortex dipole on the β-plane during one oscillation in order to clarify the transport mechanism in the meandering dipole. The dipole is initially symmetric and carries with it a finite amount of fluid (the area inside the unperturbed separatrix, see figure 1*a*). However, as the dipole moves northward, the negative vortex becomes stronger and the positive one weaker, leading to an asymmetric (instantaneous) separatrix (figure 1*b*): the area of fluid orbiting around the negative vortex becomes larger, implying that some ambient fluid has been trapped, while the area of fluid orbiting around the positive vortex becomes smaller, which means that some of the interior fluid now lies outside the separatrix and will be detrained (figure 1*c*). As the dipole returns to the initial latitude (figure 1*e*), the asymmetries in the separatrix disappear. The dipole continues travelling southwards

though, and becomes asymmetric again. Because of its larger strength, the area of fluid trapped by the positive vortex increases, while the area of the weaker negative vortex decreases (figure 1*f*). The dipole returns to its initial latitude (figure 1*h*) and the process is repeated.

Similar changes in the dipole's relative circulations and consequently in the shape of the separatrix were measured in laboratory dipoles by VFvH (see figures 6–9 of that paper). The continuous changes in relative circulation are caused by the squeezing and stretching of the fluid column in the topographic β-plane. However, the fluid depth variations have further effects: as the dipole moves uphill the distance between the two halves increases, causing entrainment of fluid, whereas when it moves downhill the dipole halves approach each other, resulting in detrainment of fluid. Figure 2 shows the entrainment and detrainment of fluid in an experimental dipole. The sequence shows qualitative similarities with the point-vortex model (figure 1), as well as some differences that will be discussed in §6.

3. Theory

The trajectory of a dipolar vortex on the β-plane can be simulated by a couple of modulated point vortices, at least for some period of time and for some range of the dipole's initial direction of propagation (see e.g. Zabusky & McWilliams 1982; VFvH). In particular, VFvH found good quantitative agreement between the model and laboratory observations when the dipole has initially an eastward component in its motion, which leads to a sine-like trajectory. This agreement was found both in the dipole trajectory and in the varying strength of the individual vortices for initial angles as high as $\frac{1}{2}\pi$ (VFvH). Therefore this simple model may be used to make quantitative estimations of mass exchange for these dipoles. On the other hand, for dipoles with a westward motion (initial angle larger than $\frac{1}{2}\pi$) the point-vortex model and the laboratory observations agree only in the perturbation enhancement mechanism and the trajectories are similar only for a short time. However, the mass exchange displayed by the point-vortex model in this interval might shed some light on the instability of the continuous dipole.

3.1. *Advection equations: a Hamiltonian system*

In the point-vortex model of a dipole (see e.g. Kono & Yamagata 1977; Zabusky & McWilliams 1982; VFvH) it is assumed that only two particles are active during the whole flow evolution and, because of conservation of potential vorticity, the circulations of these point vortices are modulated according to

$$\kappa_1 = \kappa_0 - \beta_* [\xi - \tfrac{1}{2}d(\cos\alpha_0 - \cos\alpha)], \tag{4}$$

$$\kappa_2 = -\kappa_0 - \beta_* [\xi + \tfrac{1}{2}d(\cos\alpha_0 - \cos\alpha)], \tag{5}$$

where ξ is the latitudinal coordinate of the dipole's centre and α is the direction of propagation measured from the east direction (see figure 3*a*). It is also assumed that the couple is initially symmetric (with circulations κ_0 and $-\kappa_0$) and the vortices are separated a distance d. (Note that β_* is equivalent to $\pi L^2\beta$ in VFvH, where πL^2 is the area associated with the point vortex.)

The path of the couple is described by two ordinary differential equations for the latitudinal coordinate ξ of the dipole's centre and the direction of propagation α:

$$\frac{\mathrm{d}\xi}{\mathrm{d}t} = U\sin\alpha, \quad \frac{\mathrm{d}\alpha}{\mathrm{d}t} = -\frac{\beta_*}{\pi d^2}\xi, \tag{6}$$

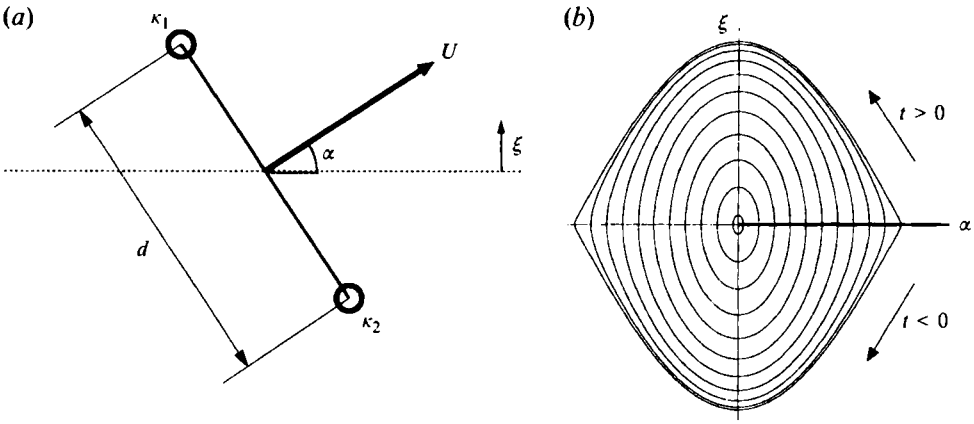

FIGURE 3. (*a*) Schematic representation of the point-vortex dipole on the β-plane. (*b*) Phase portrait α–ξ; the thick line indicates the initial conditions for an initially symmetric dipole. All solutions are time periodic, and α is an even and ξ is an odd function of time.

where
$$U = \frac{\kappa_0}{2\pi d} + \frac{\beta_*}{4\pi}(\cos\alpha_0 - \cos\alpha).$$

Figure 3(*b*) shows the periodic character (with period T) of all the solutions for an initially symmetric dipole. For the purposes of this paper it is important to notice the symmetries of the solutions. The thick line indicates the initial conditions: $\alpha = \alpha_0$ and $\xi(0) = 0$. With these initial conditions, the direction of propagation $\alpha(t)$ is an even function of time while the latitudinal displacement $\xi(t)$ is an odd function of time. Furthermore, the following relations are valid:

$$\xi(t+\tfrac{1}{2}T) = -\xi(t), \quad \alpha(t+\tfrac{1}{2}T) = -\alpha(t), \quad \kappa_1(t+\tfrac{1}{2}T) = -\kappa_2(t). \tag{7}$$

The stream function of the flow in a frame moving with the dipole is

$$\Psi = -\frac{1}{4\pi}\{\kappa_1 \ln[x^2 + (y-\tfrac{1}{2}d)^2] + \kappa_2 \ln[x^2 + (y+\tfrac{1}{2}d)^2]\} + \tfrac{1}{2}\Omega(x^2+y^2) - Uy, \tag{8}$$

where $\Omega = \partial\alpha/\partial t$. The equations describing the trajectories of fluid particles are

$$\frac{\mathrm{d}x}{\mathrm{d}t} = \frac{\partial\Psi}{\partial y}, \quad \frac{\mathrm{d}y}{\mathrm{d}t} = -\frac{\partial\Psi}{\partial x}. \tag{9}$$

This is a Hamiltonian system with Ψ playing the role of the Hamiltonian. If the flow is steady (Ψ is time independent) particle motions are integrable, the trajectories being simply the streamlines. Time-dependent flows, however, can produce chaotic particle trajectories, at least in some regions of the flow. Using the stream function given by (8) the advection equations (9) become

$$\frac{\mathrm{d}x}{\mathrm{d}t} = -\frac{1}{2\pi}\left(\frac{\kappa_1 Y_-}{I_-} + \frac{\kappa_2 Y_+}{I_+}\right) + \Omega y - U, \tag{10}$$

$$\frac{\mathrm{d}y}{\mathrm{d}t} = \frac{x}{2\pi}\left(\frac{\kappa_1}{I_-} + \frac{\kappa_2}{I_+}\right) - \Omega x, \tag{11}$$

where the definitions $Y_\pm = y \pm \frac{1}{2}d$ and $I_\pm = x^2 + Y_\pm^2$ have been used. These equations, together with the evolution equations (4)–(6), form a complete set of equations for the

study of particle trajectories in the velocity field of a meandering dipole on the β-plane. For most of the analysis that follows this form of the equations is suitable. However, for the perturbation calculations (Melnikov theory), we need to express the equations in the form of a periodically perturbed integrable Hamiltonian system:

$$\mathrm{d}x/\mathrm{d}t = f_1(x,y) + \beta_* g_1[x, y, \xi(t;\beta_*,\alpha_0), \alpha(t;\beta_*,\alpha_0)], \tag{12}$$

$$\mathrm{d}y/\mathrm{d}t = f_2(x,y) + \beta_* g_2[x, y, \xi(t;\beta_*,\alpha_0), \alpha(t;\beta_*,\alpha_0)]. \tag{13}$$

The functions f_i and g_i are given by

$$f_1 = \frac{\kappa_0}{2\pi}\left(-\frac{Y_-}{I_-} + \frac{Y_+}{I_+} - \frac{1}{d}\right), \tag{14}$$

$$f_2 = \frac{\kappa_0 x}{2\pi}\left(\frac{1}{I_-} - \frac{1}{I_+}\right), \tag{15}$$

$$g_1 = \frac{1}{2\pi}\left(-\frac{\kappa_{1\beta} Y_-}{I_-} - \frac{\kappa_{2\beta} Y_+}{I_+} + \Omega_\beta y - U_\beta\right), \tag{16}$$

$$g_2 = \frac{x}{2\pi}\left(\frac{\kappa_{1\beta}}{I_-} + \frac{\kappa_{2\beta}}{I_+} - \Omega_\beta\right), \tag{17}$$

where

$$\kappa_{1\beta} = -\xi - \tfrac{1}{2}d(\cos\alpha - \cos\alpha_0), \tag{18}$$

$$\kappa_{2\beta} = -\xi + \tfrac{1}{2}d(\cos\alpha - \cos\alpha_0), \tag{19}$$

$$\Omega_\beta = -2\xi/d^2, \tag{20}$$

$$U_\beta = -\tfrac{1}{2}(\cos\alpha - \cos\alpha_0). \tag{21}$$

This representation is exact.

3.2. *Lobe dynamics*

The use of a Poincaré map – the map of the particle location $[x(t_0), y(t_0)]$ to the location one period later $[x(t_0+T), y(t_0+T)]$ – significantly simplifies the description of particle motion in the velocity field of the meandering dipole. The map is constructed by sampling the position of a particle (relative to the dipole) every time the dipole returns to its initial configuration, i.e. every time $\xi = 0$ and $\alpha = \alpha_0$.

The streamline patterns of the stationary flow (i.e. for $\beta_* = 0$, but also for $\alpha_0 = 0, \pi$) are illustrated in figure 4(*a*). There exist two fixed points p_+ and p_- corresponding to the front and rear stagnation points of the dipole, respectively. Both are of hyperbolic type so that there is a collection of orbits forming a line that approaches p_- as $t \to +\infty$, called the *stable manifold*, and a collection of orbits that emanates from p_+ (i.e. approaches p_+ as $t \to -\infty$), called the *unstable manifold*. In the unperturbed case the unstable manifold of p_+ and the stable manifold of p_- coincide and correspond to the separatrix. There are additionally two elliptic fixed points corresponding to the positions of the point vortices. The separatrix divides the flow in three regions: the free flow region, where particles simply move from the right to the left along the open streamlines; the positive-vortex core where particles rotate anticlockwise; and the negative-vortex core where the particles rotate clockwise. The particles in the cores are trapped and travel permanently with the dipolar vortex.

For $\beta_* \neq 0$ but sufficiently small the fixed points persist and the unstable manifold of p_+ smoothly emanates from p_+ as before, but in this case undergoes strong oscillations as it approaches p_-. Similarly, the stable manifold of p_- smoothly emanates from p_- but undergoes strong oscillations as it approaches p_+. The structure that results from the intersection of the manifolds of the two hyperbolic points is called a

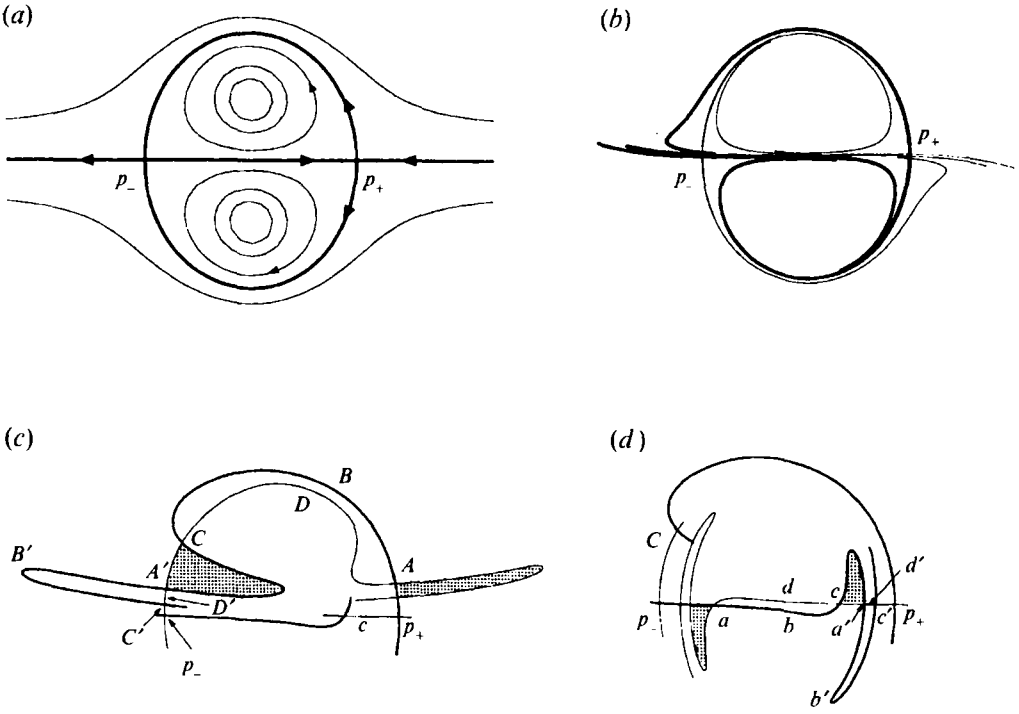

FIGURE 4. (*a*) Streamlines of an unperturbed point-vortex dipole. (*b*) The heteroclinic tangle in the perturbed case. The thick line represents the unstable manifold of p_+ and the thin line the stable manifold of p_-. (*c*) The mechanism for transport between the cyclonic vortex and the ambient fluid: region $ABCD$ is mapped to $A'B'C'D'$ (see text). (*d*) Transport between the two dipole halves: region $abcd$ is mapped to $a'b'c'd'$ (see text).

heteroclinic tangle, see figure 4(*b*), which shows the heteroclinic tangle for $\beta_* = 0.2$ and $\alpha_0 = 0.318\pi$. The three regions identified in the unperturbed case persist in a reduced form but the new limit between them is not a line but a 'chaotic sea' or mixing region.

The intersecting manifolds expose the mechanism for transport of fluid between the *interior* and the *exterior* of the vortex dipole, where interior and exterior are yet to be defined for the perturbed case. Usually, the definition that best approximates the unperturbed case is chosen. However, for a dipole on a β-plane any choice greatly differs from the symmetric separatrix (compare figures 4*a* and 4*c*). Let A and C be two adjacent intersections between the stable and unstable manifolds, and B a point on the unstable manifold and D a point on the stable manifold, as indicated in figure 4(*c*). If one chooses the boundary between the cyclonic vortex and the ambient fluid as the line formed by p_+C on the unstable manifold of p_+, and Cp_- on the stable manifold of p_-, then a large fraction of fluid initially located out of the dipole is included as interior fluid. On the other hand, a large fraction of fluid initially located in the dipole is excluded from the vortex if the boundary is chosen as the line p_+A on the unstable manifold of p_+, and Ap_- on the stable manifold of p_-. With the use of the first definition, the area $ABCD$ in figure 4(*c*), which maps to the area $A'B'C'D'$, represents the fluid that will be detrained from the cyclonic vortex in the next cycle; whereas the dotted area near A, which maps to the dotted area near A', represents the fluid that will be entrained. Since the flow is incompressible, the area entrained is equal to the area detrained in every cycle. The overestimation of detrainment produced with the adopted definition of the boundary is corrected with the use of an *effectively detrained area*,

which is simply the intersection of the detrainment lobe with the area enclosed by the unperturbed separatrix.

Similarly, the tangle formed by the unstable manifold of p_- and the stable manifold of p_+ gives rise to transport of fluid between the cyclonic and the anticyclonic halves of the dipolar vortex (figure 4*d*). In this case the area *abcd* is mapped to *a'b'c'd'*, i.e. moves from the cyclonic half to the anticyclonic one; and the same amount of fluid (the dotted area close to *a*) leaves the anticyclonic vortex half and enters the cyclonic one.

The unstable manifold is numerically constructed by computing the evolution of a small line located on the fixed point forward in time. This line will be stretched in the direction of the unstable manifold. Here we have used a straight line of length $0.1d$ (with d the distance between the point vortices) placed perpendicularly to the symmetry axis of the dipole; the use of different lengths or orientations of the line leaves the lobe area unchanged within 0.5%. The stable manifold is constructed in a similar way, but the integration is now backwards in time. A fourth-order Runge–Kutta scheme was used for the time integration. New nodes were added during the integration, the new positions being computed with cubic splines between smooth segments of the line. The exchange of mass can be evaluated directly from the discrete set of points defining the manifolds. Once a single lobe is identified the area follows from $\mu = \oint x\,\mathrm{d}y$ along *ABC–CDA*. This method is valid for every amplitude of perturbation β_*.

3.3. *Melnikov theory*

Without explicitly solving the advection equations (10) and (11), it is possible to predict the behaviour of the stable and the unstable manifolds using the *Melnikov function*. This function is, up to a known normalization factor, the first-order term in the Taylor expansion about $\beta_* = 0$ of the distance between the stable and the unstable manifolds. The Melnikov function $M(t_0)$ is defined as

$$M(t_0) = \int_{-\infty}^{\infty} \{f_1[\boldsymbol{x}_u(t)]\, g_2[\boldsymbol{x}_u(t), \xi(t+t_0;\beta_*,\alpha_0), \alpha(t+t_0;\beta_*,\alpha_0)] - f_2[\boldsymbol{x}_u(t)]\, g_1[\boldsymbol{x}_u(t), \xi(t+t_0;\beta_*,\alpha_0), \alpha(t+t_0;\beta_*,\alpha_0)]\}\,\mathrm{d}t, \quad (22)$$

where $\boldsymbol{x}_u(t) = (x_u(t), y_u(t))$ represents the particle trajectory along the separatrix of the unperturbed dipole. The Melnikov theorem shows that a simple zero of $M(t_0)$ implies a transverse intersection of the stable and the unstable manifolds (see e.g. Rom-Kedar *et al.* 1990), while one intersection implies the existence of infinitely many intersections of the manifolds (i.e. a *heteroclinic tangle*). This heteroclinic tangle gives rise to horseshoe maps and forms therefore the underlying mechanism for chaotic particle motion (see e.g. Rom-Kedar *et al.* 1990). The Melnikov function therefore yields a specific criterion for the existence of chaotic particle trajectories in terms of the system parameters (α_0 and β_* in our case).

One can also obtain an $O(\beta_*)$ approximation for the area of a lobe by using the Melnikov function (Rom-Kedar *et al.* 1990). The area of a lobe is given by

$$\mu = \beta_* \int_{t_{01}}^{t_{02}} M(t_0)\,\mathrm{d}t_0 + O(\beta_*^2), \quad (23)$$

where t_{01} and t_{02} are two adjacent zeros of the Melnikov function $M(t_0)$ (i.e. they correspond to adjacent intersections of the unstable and stable manifolds).

The Melnikov function (22) and the lobe area (23) were computed numerically in the following way. (i) The trajectory along the unperturbed separatrix $\boldsymbol{x}_u(t)$ and the equations of motion (6) were integrated using a fourth-order Runge–Kutta scheme; (ii)

the velocity fields $f_i(t)$ and $g_i(t)$ were calculated using the results of (i); and (iii) the integrals were evaluated using the trapezoidal rule. The infinite limits of the integral in (22) were replaced by large but finite limits (large means here that the use of a larger value leaves the integral unaffected).

Some symmetries

Note that if the particle trajectory along the separatrices is chosen in such a way that $x_u(t=0)=0$ (i.e. $t=0$ at the intersection of the heteroclinic trajectory with the y-axis), the following symmetries hold for the time-independent components of the velocity field:

$$f_1[x_u(t)] = f_1[x_u(-t)],$$
$$f_2[x_u(t)] = -f_2[x_u(-t)].$$

Then the Melnikov function $M(t_0)$ is equal to zero for all $t_0 = t_0^*$ such that the time-periodic components of the velocity field have the same symmetry with respect to t_0^*:

$$g_1[x_u(t), t_0^*+t] = g_1[x_u(-t), t_0^*-t],$$
$$g_2[x_u(t), t_0^*+t] = -g_2[x_u(-t), t_0^*-t].$$

These symmetries are satisfied if $\xi(t_0^*+t) = \xi(t_0^*-t)$ and $\alpha(t_0^*+t) = \pm\alpha(t_0^*-t)$, as can be seen in equations (18)–(21). Thus t_0^* must correspond to an extreme latitudinal displacement in the motion of the dipole. In general $t_0^* = \frac{1}{2}(n+\frac{1}{2})T$ for n an integer and T the period of the dipole's meandering motion. $M(t_0)$ has thus an infinite number of isolated zeros, two for every period of the perturbation.

4. Numerical results for strength perturbations

4.1. *Entrainment and detrainment*

The area enclosed by one dipole half has been chosen as the unit area for the evaluation of the mass exchange; therefore, a lobe that occupies say 10% of the cyclonic vortex has an area $\mu = 0.1$ in our arbitrary system. Figure 5 shows the detrainment lobe (of the cyclonic half) for constant $\alpha_0 = 0.318\pi$ and increasing $\beta_* =$ (*a*) 0.04, (*b*) 0.08, (*c*) 0.12, (*d*) 0.16 and (*e*) 0.2. The lobe is thin and long for small β_* and reduces in length and increases in thickness with increasing β_*. The area of the lobe increases with β_*, but it occupies regions close to the unperturbed separatrix of the cyclonic half, indicating that a large portion of the core will remain trapped by the vortex. Similarly, figure 5 also shows the detrainment lobe for constant $\beta_* = 0.1$ and increasing initial orientation angles $\alpha_0 \approx$ (*f*) 0.127π, (*g*) 0.254π, (*h*) 0.381π, (*i*) 0.508π and (*j*) 0.635π. The lobe increases in length and in thickness with increasing α_0. Obviously the lobe area also increases. The lobe now 'penetrates' closer to the positive point vortex, thus reducing the size of the positive core.

Figure 6(*a*) shows the amount of fluid μ exchanged between the cyclonic half and the ambient fluid during one oscillation of the dipole computed using the Melnikov function. The initial angle is varied from 0 to π, and β_* is varied in the range 0–0.3. The area of the lobe increases with both increasing β_* and α_0. The area is zero for $\alpha_0 = 0$: this initial condition corresponds to the stable equilibrium (ETD) and no change of circulation occurs in the couple, and therefore no change of the shape of the separatrix. For $\alpha_0 \to \pi$ the area of the lobe does not go to zero, since $\alpha_0 = \pi$ corresponds to the unstable equilibrium. The area of the lobe tends to a finite value which depends on β_*. For $\beta_* = 0$ the lobe area is also zero because then there is no variation of the circulation of the vortices, independently of the direction of propagation.

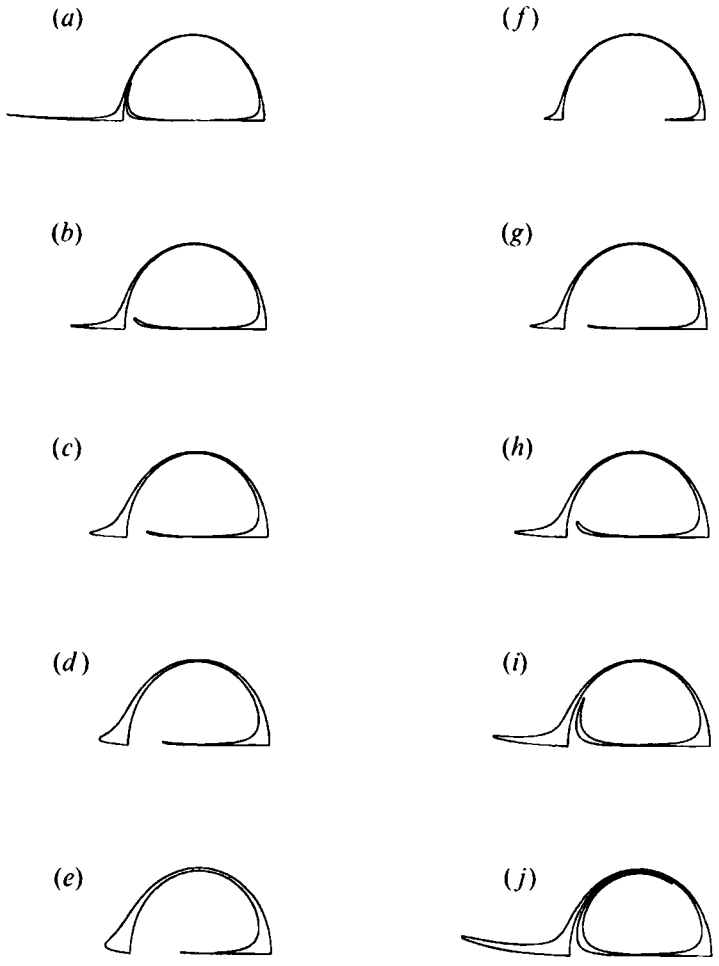

FIGURE 5. The detrainment lobe of the cyclonic dipole half for constant $\alpha_0 = 0.318\pi$ and (*a*) $\beta_* = 0.04$, (*b*) 0.08, (*c*) 0.12, (*d*) 0.16 and (*e*) 0.2. The detrainment lobe for constant $\beta_* = 0.1$ and (*f*) $\alpha_0 \approx 0.127\pi$, (*g*) 0.254π, (*h*) 0.381π, (*i*) 0.508π and (*j*) 0.635π.

Figure 6(*b*) shows the exchange rate μ^* (i.e. the amount of fluid that is exchanged per unit time) between the cyclonic half and the ambient fluid. This rate is obtained by dividing the lobe area (figure 6*a*) by the period of the dipole's oscillation (i.e. the perturbation period). The rate is zero for $\beta_* = 0$ and for $\alpha_0 = 0$, where the lobe area is zero, but also for $\alpha_0 = \pi$, where the period of the oscillation goes to infinity. Therefore, for every value of $\beta_* \neq 0$ the exchange rate has a maximum and this occurs at the same value of $\alpha_0 \approx 0.62\pi$, within the resolution of our calculations.

The sections $\alpha_0 = 0.318\pi$ and $\beta_* = 0.1$ in the parameter plane have been chosen to compare the results of Melnikov calculations and the area of the lobe computed by direct numerical integration of (10) and (11). Both methods agree very well, as they should, for small values of both β_* and α_0 (figures 7*a*, *c*). For larger values the Melnikov function underestimates the amount of fluid that is detrained. The exchange rate increases in a linear manner with β_* (figure 7*d*) and shows a maximum for $\alpha_0 \approx 0.62\pi$ (figure 7*b*). Both methods show this maximum although they are slightly shifted, the one from direct numerical integration occurring for a greater value of α_0.

The total exchange and the exchange rate between the negative vortex and the

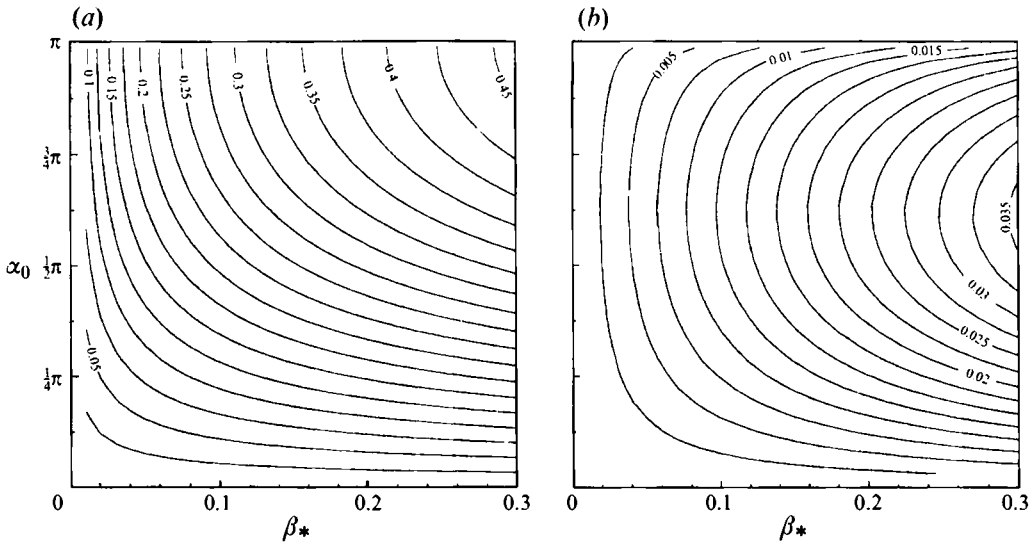

FIGURE 6. (*a*) Area (μ) of the lobe detrained from the cyclonic half to the ambient fluid computed using the Melnikov function. Contour interval 0.025, μ is zero along both axes. (*b*) Exchange rate $\mu^* = \mu/T$ (where T is the period of the dipole's meandering motion). Contour interval 0.005.

ambient fluid are exactly the same as those described above for the positive vortex. Because of the symmetries (7) the manifolds in the Poincaré section $t = 0$ are the mirror image with respect to the x-axis of the manifolds in the Poincaré section $t = \frac{1}{2}T$. The exchange of mass between the two dipole halves shows the same qualitative behaviour as the exchange with the ambient fluid. The numerical calculations have revealed an approximate quantitative relation between them: $\mu_U = (1.585 \pm 0.025)\mu_M$, where μ is the area of the lobe and the subindexes U, M indicate exchange with the ambient fluid (through the upper separatrix) and between the two dipole halves (through the middle separatrix), respectively.

Figure 7 also shows the effective area of fluid (μ_E) detrained during the first period of the dipole's meandering motion. This area is simply the intersection of the detrainment lobes (as illustrated in figure 5) and the unperturbed separatrix (figure 4*a*). Approximately 50% of the detrainment lobe lies within the initial separatrix. For the range of parameters studied here the following relation has been found: $\mu_E = (0.49 \pm 0.01)\mu$.

The amount of fluid detrained in one period does not depend on the period as it does in the case of a vortex pair in an oscillating strain flow studied by Rom-Kedar *et al.* (1990). The most likely reason is that on the β-plane the perturbation period is, for the parameter range studied in this paper, much larger than the typical time scale of dipole propagation: the length of the dipole's trajectory during one oscillation is at least several times the distance between the point vortices.

Here the dominant factor is the amplitude of the perturbation, measured by the term $\beta_* A$, where A is the amplitude of the latitudinal displacement. The fluid area detrained in the first period is given by

$$\mu_E = (0.32 \pm 0.01)\beta_* A. \tag{24}$$

This result can be understood in the following way: the amount of detrained fluid should be related to the difference S_1 between the area enclosed by the unperturbed separatrix and the area enclosed by the separatrix at the position of maximal

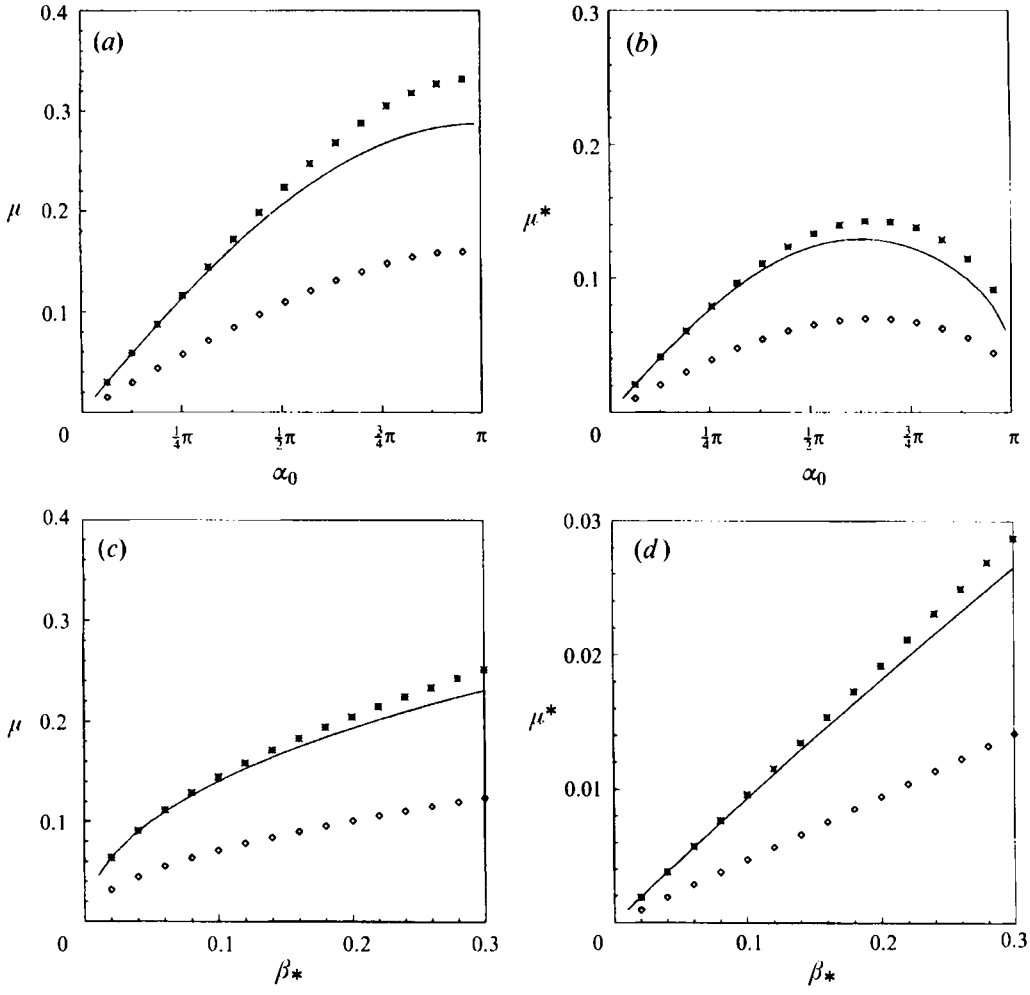

FIGURE 7. Lobe area (μ) and exchange rate (μ^*) computed using the Melnikov function (solid line), and direct numerical integration of the advection equations (asterisks). $\beta_* = 0.1$ for (a) and (b); $\alpha_0 = 0.318\pi$ for (c) and (d). The diamonds indicate the 'effectively detrained area' (see text).

asymmetry of the dipole (figure 8a). If the perturbation period is of the same order or greater than the orbit period 'close' to the separatrix, then most of the fluid located outside the current separatrix is advected to the dipole's wake. In contrast, a significant portion of this fluid is recaptured during the same oscillation of the dipole when the perturbation period is small.

The shape of the separatrix depends on the ratio $\epsilon = -\kappa_2/\kappa_1$ and the distance between the vortices d, which is constant. S_1 has been computed numerically as a function of ϵ and it has been found to be given by $S_1 \approx 0.15\,(\epsilon - 1)$ for $1 < \epsilon < 2$ (figure 8b). On the β-plane the extreme values of ϵ are reached at the position of maximum displacement in the latitudinal direction, and the most important term in determining the amplitude of the strength's perturbation is $\beta_* A$, as can be deduced from (4) and (5). The ratio between the circulations becomes $\epsilon \approx 1 + 2\beta_* A$, leading to $S_1 \approx 0.3\beta_* A$. The latter relation compares very well with (24).

The same argument explains the almost constant ratio between the amount of fluid exchanged by the two dipole halves and the fluid exchanged between one half and

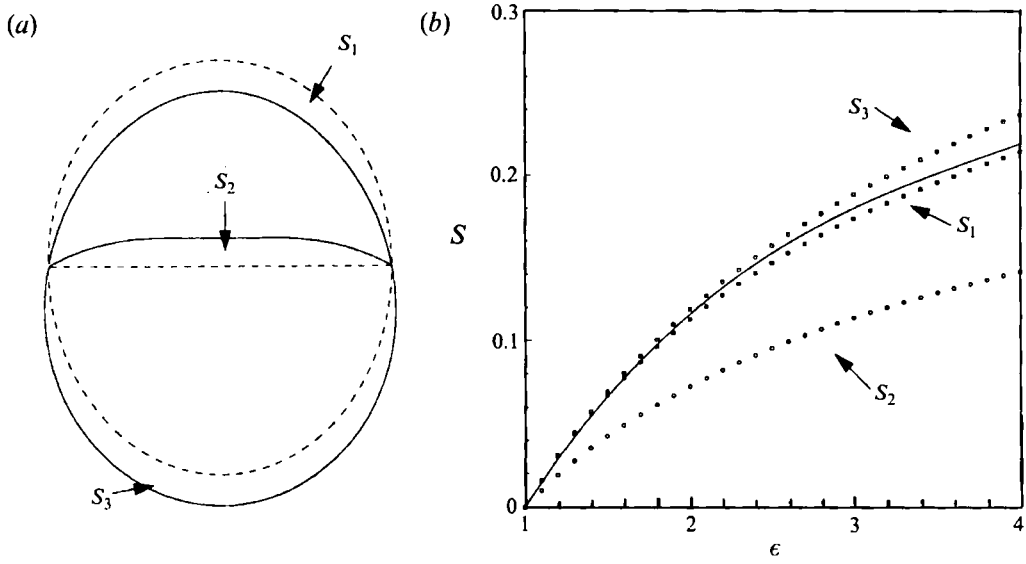

FIGURE 8. (*a*) The areas S_1, S_2 and S_3 are part of the open flow, the cyclonic core or the anticyclonic core, depending on whether the dipole is symmetric (broken line) or asymmetric (solid line). (*b*) S_1, S_2 and S_3 as functions of the asymmetry of the dipole $\epsilon = -\kappa_2/\kappa_1$; the line is an approximation given by $S = 0.15(\epsilon-1)+0.04(\epsilon-1)^2+0.005(\epsilon-1)^3$.

the ambient fluid (1.585 ± 0.025 according to the Melnikov function calculations). Numerical computations using the asymmetric separatrices give a ratio of $S_1/S_2 = 1.6$ (see figure 8).

4.2. *Long time spread of particles*

In the previous section we evaluated the amount of fluid (lobe area) that is exchanged between different regions of the flow in one period of the meandering dipole. The specific fluid area that undergoes such a process was also determined (i.e. the detrainment lobe). In this section we explore the evolution of particles for longer periods. We discuss three cases: (*a*) a dipole with wave-like motion and net eastward drift ($\alpha_0 = 0.159\pi$), (*b*) a dipole moving along an 8-shaped path and zero net drift ($\alpha_0 = 0.713495\pi$), and (*c*) a dipole with cycloid-like motion and net westward drift ($\alpha_0 = 0.796\pi$). The choice is motivated by one important difference between these cases: in (*a*) the dipole travels indefinitely in the eastward direction without ever returning close to its initial position, in (*b*) the dipole returns periodically to its initial position, and therefore fluid that was detrained can be recaptured by the dipole in a later passing, and in (*c*) there is a series of points through which the dipole passes twice.

Particles were initially placed on a regular array within the detrainment lobe of the positive vortex ('yellow' particles) and the negative vortex ('green' particles), and their positions were sampled at times nT, where n is an integer and T is the period of the dipole's meandering.

In the wave-like mode (figure 9*a*) the dipole simply leaves a very thin and long tail along the meandering path. In case (*b*) one observes alternating bands of ambient and interior fluid, and the particles are spread in the latitudinal and in westward directions over distances larger than the scale of the trajectory of the dipole itself (indicated by a white line in figure 9*b*). There is a net westward transport of fluid in spite of the dipole's zero drift. This can be understood in the following way. As the dipole moves northward, the positive vortex (which occupies the west side of the couple) becomes

(a)

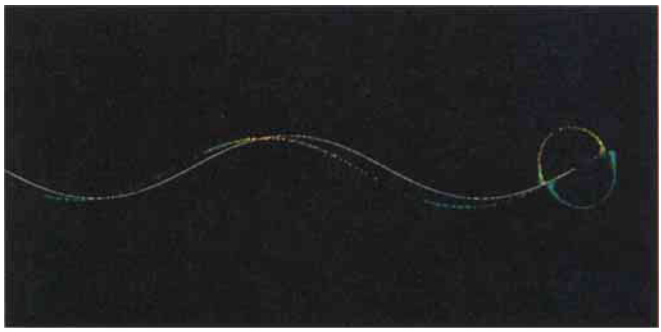

(b)

(c)

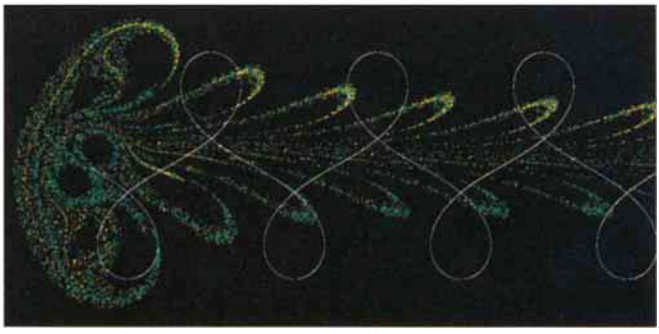

FIGURE 9. Positions of fluid particles at $t = nT$, where T is the dipole's oscillation period and n is an integer number. The yellow particles were originally located within the detrainment lobe of the cyclonic dipole half and the green particles within that of the negative half. The white line represents the dipole's trajectory. (*a*) A dipole in the wave-like regime ($\alpha_0 = 0.159\pi$); $n = 0, 1, 2, 3$. (*b*) The 8-shaped trajectory with zero net zonal drift ($\alpha_0 = 0.713495\pi$); $n = 1, \ldots, 9$. (*c*) A dipole in the cycloid-like regime ($\alpha_0 = 0.796\pi$), $n = 1, \ldots, 6$.

weaker and detrains fluid, while the negative vortex (which occupies the east side) becomes stronger and entrains fluid. On the other hand, as the dipole moves southward, the negative vortex (on the west side of the couple) becomes weaker and detrains fluid, while the positive vortex (on the east side) becomes stronger and entrains fluid. In both cases the vortex located on the east entrains fluid while the vortex located on the west detrains fluid, resulting therefore in a net mass transport in the westward direction. Finally, in the cycloid-like mode, some particles are left behind in the form of large lobe structures, while other particles form a kind of front that advances in the westward direction (figure 9*c*). It can also be observed that the stable cores (the regions around the point vortices) decrease in size as the tilting angle increases.

5. Size perturbations

The meandering trajectory of a dipolar vortex on a topographic β-plane causes the water column to be alternately stretched and squeezed. As a result the distance between the vortex centres will decrease as the dipole moves into deep water and increase as the dipole moves towards shallower water (see figure 11 in VFvH). This process is periodic (with the same period as the variation of the vortices' strengths) and leads to entrainment of fluid during the 'expanding' phase of the dipole and detrainment of fluid during the 'shrinking' phase.

This effect is modelled using the point-vortex dipole with constant circulation κ_0 and $-\kappa_0$, respectively, but imposing on it a sine-like variation of the distance between the vortices:

$$d = d_0(1 + \epsilon_d \sin \omega t), \tag{25}$$

where d_0 is the initial distance between the vortices (as the dipole is located at its equilibrium latitude). The frequency ω is the frequency of the meandering motion on the β-plane and for simplicity it will be taken as in the linear approximation of VFvH (see the solution of equation (2.7) in that paper). The amplitude of the size perturbation ϵ_d is related to the parameters of the topographic β-plane in the following manner. The depth of the fluid is given by $h = h_0(1 - sy)$, and by conservation of volume the radius of a column of fluid moving on this topography is given by $r = r_0(1 - s\xi)^{-1/2} \approx r_0(1 + \frac{1}{2}s\xi)$. This relation is assumed to hold for the variation of the distance between the two point vortices. In the linear approximation, the latitudinal position of the dipole's centre is given by $\xi = A \sin \omega t$, where A is the maximum latitudinal displacement. This leads to the following expression for the frequency ω and the amplitude ϵ_d of the size perturbation:

$$\omega = (\beta_* U_0/\pi d^2)^{1/2}$$

$$\epsilon_d = \tfrac{1}{2}sA = \beta A/(4\Omega_E).$$

Because of the symmetry about the x-axis we only need to examine the transport across the upper separatrix. Transport across the lower manifold is the same. The middle separatrix does not break up and therefore no exchange of fluid can occur between the two halves of the vortex dipole.

The advection equations for the point-vortex dipole with varying size can be written in the form of a periodically perturbed integrable Hamiltonian system:

$$\mathrm{d}x/\mathrm{d}t = f_1(x, y) + \epsilon_d g_1(x, y, t; \omega) + O(\epsilon_d^2),$$

$$\mathrm{d}y/\mathrm{d}t = f_2(x, y) + \epsilon_d g_2(x, y, t; \omega) + O(\epsilon_d^2)$$

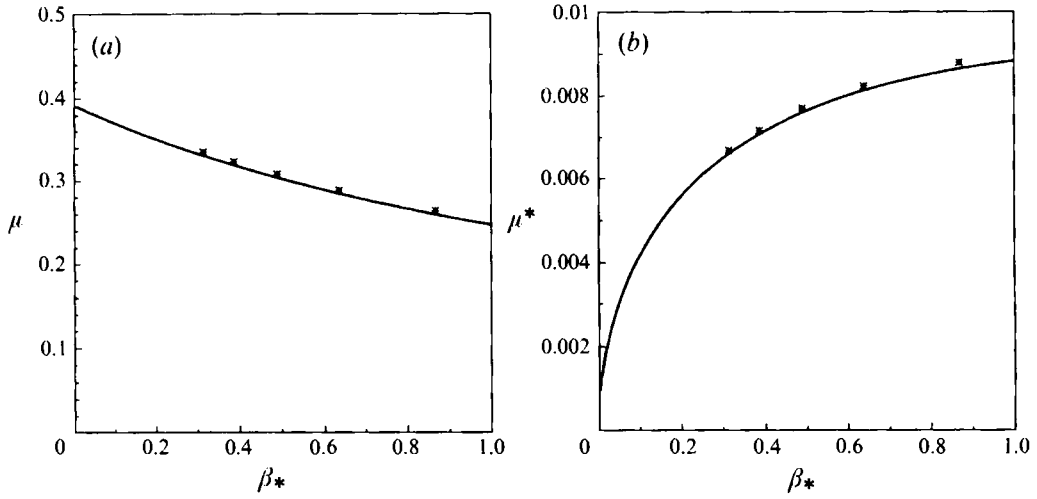

FIGURE 10. Transport in the point-vortex dipole with oscillating size: (*a*) lobe area μ, and (*b*) exchange rate μ^* as a function of β_*. The solid line shows the Melnikov function, and the asterisks the direct numerical integration of the advection equations.

by substituting the value of d given by (25) in (10) and (11) and making a Taylor expansion of these equations around d_0.

The functions f_i are the same as in the β-plane perturbations, see (14) and (15), and g_i are now given by

$$g_1 = \frac{\sin \omega t}{4\pi}\left(\frac{x^2 - Y_-^2}{I_-^2} + \frac{x^2 - Y_+^2}{I_+^2} + 2\right), \tag{26}$$

$$g_2 = \frac{x \sin \omega t}{2\pi}\left(\frac{Y_-}{I_-^2} + \frac{Y_+}{I_+^2}\right). \tag{27}$$

Defining $g_i = g_i^* \sin \omega t$, and using the symmetries present in the equations [f_1, $Y_\pm$ and $I_\pm$ are even, and f_2 and x are odd functions of t for the choice $x_u(t = 0) = 0$], the Melnikov function becomes

$$M(t_0) = \cos \omega t_0 \int_{-\infty}^{\infty} \{f_1[\boldsymbol{x}_u(t)]\, g_2^*[\boldsymbol{x}_u(t)] - f_2[\boldsymbol{x}_u(t)]\, g_1^*[\boldsymbol{x}_u(t)]\} \sin \omega t \, \mathrm{d}t. \tag{28}$$

The integral is a function of β_* through the dependence on ω and therefore will be denoted by $F(\beta_*)$, which is non-zero for the parameter region studied in this paper ($0 < \beta_* < 0.3$). $M(t_0)$ has therefore an infinite number of simple zeros (i.e. $M(t_0) = 0$ and $\partial M(t_0)/\partial t_0 \neq 0$) for every point in the parameter space.

In figure 10 the solid line represents lobe area computed using the Melnikov function and the markers show the lobe areas obtained from direct numerical integration of the advection equations for $\epsilon_d = 0.1$. Different values of ϵ_d produce a similar curve, but with the lobe areas being some multiple of the ones shown here.

The lobe area decreases with increasing β_*. This is because the period also decreases with β_*, and a shorter period allows less fluid to be exchanged. However, this behaviour changes for the *exchange rate* (mass exchanged per unit of time). The exchange rate is maximal where $\omega F(\beta_*)/2\pi$ is maximal. This maximum is reached for $\beta_* = 1.8 \pm 0.1$.

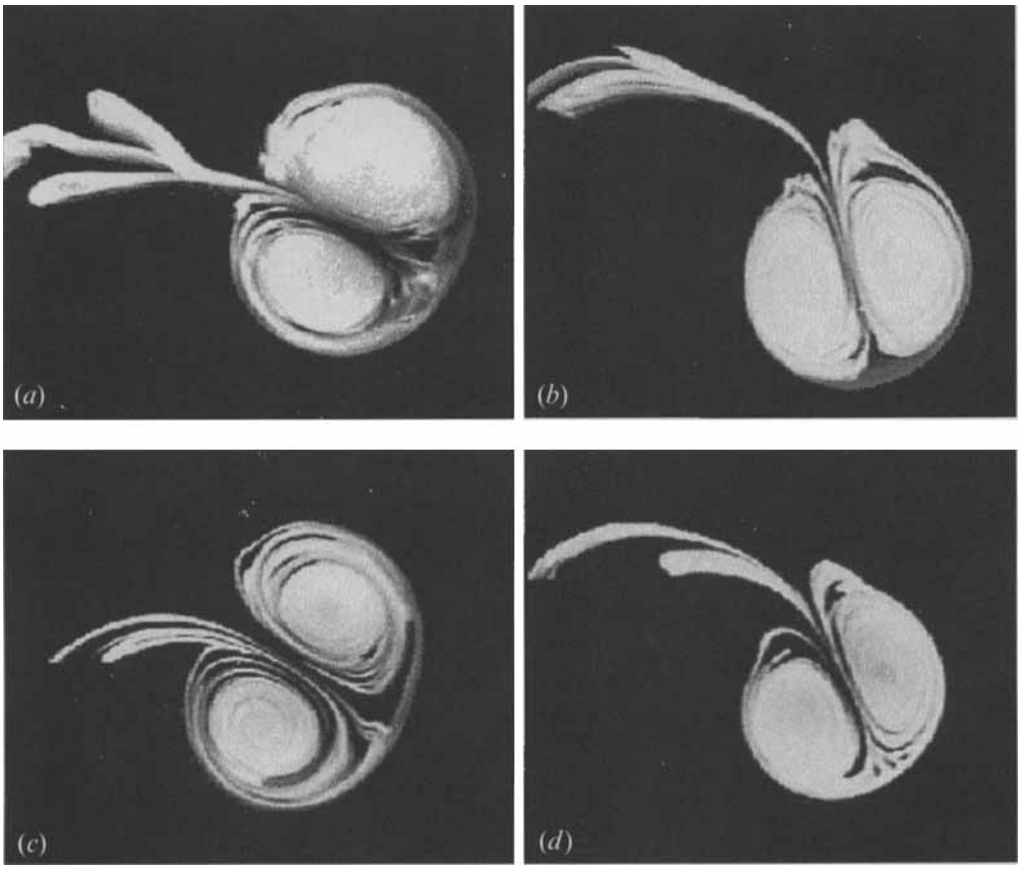

FIGURE 11. Experimental images showing the formation of lobe-like structures after half a period of the dipolar motion for different initial direction of propagation and gradient of ambient vorticity: (*a*) $\alpha_0 = \frac{1}{4}\pi$, $\beta = 0.194\ \mathrm{m^{-1}\ s^{-1}}$, (*b*) $\alpha_0 = \frac{1}{2}\pi$, $\beta = 0.194\ \mathrm{m^{-1}\ s^{-1}}$, (*c*) $\alpha_0 = \frac{1}{4}\pi$, $\beta = 0.344\ \mathrm{m^{-1}\ s^{-1}}$, (*d*) $\alpha_0 = \frac{1}{2}\pi$, $\beta = 0.344\ \mathrm{m^{-1}\ s^{-1}}$.

6. Experimental observations

In this section we present results of flow visualizations and compare them with numerical simulations. Four combinations of the parameter values $\beta = 0.194$, $0.344\ \mathrm{m^{-1}\ s^{-1}}$ and $\alpha_0 = \frac{1}{4}\pi, \frac{1}{2}\pi$ were used.

In figure 11 the dipolar structures are shown after one half of the oscillation, when they have returned to their equilibrium latitude. Figure 11(*a*, *c*) shows broad dipolar structures, which were started at an angle $\alpha_0 = \frac{1}{4}\pi$. At this stage, undyed fluid is entrained at the rear side, advected to the front side along the dipole's symmetry line and then wrapped around each dipole half parallel to the boundary of the dipole (the separatrix). It is also possible to observe thin spiral structures close to the vortex centres, but these patterns were formed during the generation of the dipole and therefore they are not related to the entrainment–detrainment mechanism discussed here. The different origin of the various patterns shown here are best observed in the video recordings of the experiments. For $\beta = 0.344\ \mathrm{m^{-1}\ s^{-1}}$ the dipole shows also a lobe structure that is being advected with the long tail (figure 11*c*).

Figure 11(*b*, *d*) shows dipoles with initial direction of propagation $\frac{1}{2}\pi$. The dipoles are now more compact than those with initial direction of propagation $\alpha_0 = \frac{1}{4}\pi$. The

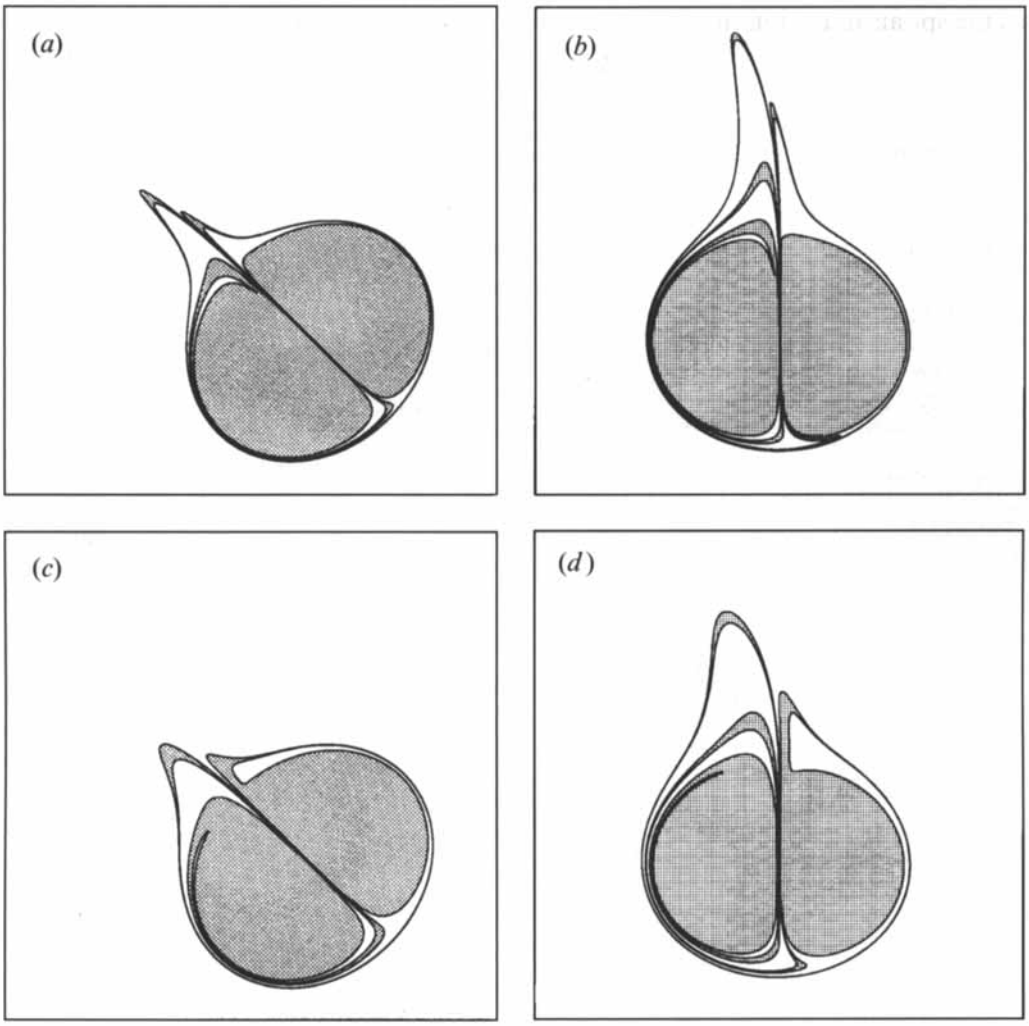

FIGURE 12. The same as in figure 11 but now for numerical simulations using the modulated point-vortex model. The hatched areas correspond to fluid initially trapped by the point-vortex dipole.

spiral structure of ambient fluid is thinner, showing that little fluid has been entrained; and larger lobes of interior fluid are left behind, especially for $\beta = 0.344\ \mathrm{m^{-1}\ s^{-1}}$ (figure 11*d*).

In figure 12 the corresponding numerical simulations are shown. Both strength and size perturbations (4)–(5) and (25) are used in the advection equations. The parameter values and initial conditions approximately match the values used in the experiments (figure 11). A fluid patch limited by the unperturbed separatrix has been followed during one half of the perturbation period.

Figure 12(*a*) shows two thin lobes, each one originating from a dipole half, and a second lobe is being formed in the anticyclonic vortex. Ambient fluid has been entrained but it is confined to a thin layer close to the original separatrix, indicating that large cores of interior fluid remain trapped by the dipole. On the rear as well as on the front side of the dipole the 'interior' and the 'exterior' fluid are located in alternating bands, the ones formed by exterior fluid being thicker.

Figure 12(*c*) shows essentially the same feature as figure 12(*a*) but the lobes as well

as the spirals in the interior of the dipole are thicker. These structures are in an earlier stage of their evolution because now the period is shorter than in figure 12(*a*). The dipoles in figure 12(*b*, *d*) show the same characteristic features and mutual differences as the dipoles in figure 12(*a*, *c*). Note, however, that a third lobe-like structure appears in the anticyclonic vortex.

Qualitatively, similar features can be recognized such as entrainment and detrainment of fluid through the formation of lobes and spiral structures. Note that the long tail in the experiment is formed during the generation of the dipolar vortex (see VFvH) and is not a result of the perturbations in strength or size. Another difference is that the experimental dipoles with a greater eastward component ($\alpha_0 = \frac{1}{4}\pi$) have a net growth and therefore there is mainly entrainment of fluid and hardly any fluid is detrained. The growth of the eastward propagating dipoles is caused by the generation of relative vorticity in the dipoles exterior (see VFvH); this secondary vorticity field gives rise to a shear that might be the cause of the large lobe in the cyclonic vortices (figure 11*b*, *d*).

7. Conclusions

Mass transport during the meandering motion of a dipolar vortex on the β-plane is investigated. The meandering motion occurs if the dipole travels transversally to lines of equal ambient vorticity. Owing to conservation of potential vorticity the relative vorticity of the dipole changes asymmetrically, resulting in alternately net positive and negative circulation. The stream function pattern changes accordingly, thus providing the possibility for fluid to escape or enter the dipolar structure.

The modulated point-vortex dipole models this basic mechanism appropriately (see e.g. Kloosterziel *et al.* 1993; VFvH). This model is therefore used to study the transport of mass between different regions of the flow during the meandering motion of the dipole. The equations of motion of passive tracers are shown to have the form of a periodically perturbed integrable Hamiltonian system. The time-independent part of the stream function is that of the symmetric vortex couple with constant circulations, and the time-periodic component corresponds to that of a couple of point vortices of the same sign, but with varying intensities.

Recent techniques of the theory of transport in dynamical systems (so-called lobe dynamics, see Rom-Kedar *et al.* 1990) are applied to calculate the amount of fluid that is entrained and detrained in every period of the dipole's meandering motion as well as the rate at which this interchange takes place. These quantities are computed as a function of the initial direction of propagation α_0 and the gradient of ambient vorticity β. The amount of mass exchanged increases with increasing β and increasing α_0 and it is approximately proportional to the product βA. The exchange rate has a maximum for $\alpha_0 \approx 0.62\pi$ for every value of β.

On a topographic β-plane the changes in relative vorticity are caused by squeezing of the fluid column as the dipole moves uphill and stretching as the dipole moves downhill. These processes induce a periodic change in the distance between the points where the extreme values of vorticity occur, thus leading to detrainment as the points approach each other and entrainment of fluid as the points move apart. The exchange of mass due to this mechanism is studied independently using a symmetric point-vortex couple separated by a distance that changes periodically in time. For equal amplitudes of perturbation (i.e. the same percentage variations with respect to the unperturbed value), the size variation causes more exchange of fluid than the variation of strength.

The point-vortex model is compared with experimental observations for a few points

in the parameter space. The deformation of the initial separatrix is computed numerically using both modulation of the vortices circulations and oscillation of the distance between the point vortices. The comparison is made after the dipole returns to its equilibrium latitude (isobath), i.e. after one half of the perturbation period. Good qualitative agreement exists in the main features: formation of spiral structures of ambient (undyed) fluid in the interior of the dipole and lob-like (dyed) structures left behind in the wake of the dipole. The main differences are that the dipoles with a greater eastward component grow in the experiment (and therefore there is mainly entrainment of fluid) and that larger lobes are formed in the experimental dipoles than in the simulations. The observed differences are most likely due to the absence of relative vorticity generation in the point-vortex model. As discussed in VFvH this secondary vorticity field is responsible for the expansion of dipolar vortices with an eastward component and also causes a shear flow, which could also promote the shedding of mass.

The results obtained with the point-vortex model are expected to give a good estimate of the mass exchange in the continuous case for the same parameter interval where the trajectories behave in a similar way, i.e. for tilting angles less than $\frac{1}{2}\pi$ (see VFvH). The small mass exchange observed in this region indicates that the eastward travelling dipole, besides having a stable trajectory, preserves its mass identity for long time. On the other hand, the westward travelling dipole, which has an unstable trajectory in the point-vortex model as well as in the experiments, loses a large fraction of its mass according to the model. This mass loss also represents, in the continuous case, loss of vorticity and leads therefore to the destruction of the dipolar structure.

Without explicitly computing the mass exchange, Hobson (1991*a*) concluded, from the structure of the heteroclinic tangles, that the mass exchange should increase with the tilting angle. In the discussion of the implications of this result for an atmospheric blocking – thought to be a WTD which remains stationary due to the eastward circulation – Hobson (1991*a*) concluded that this disturbance does not form a complete barrier for mass transport. This may be true, but it cannot be concluded from the point-vortex model, which shows that the exchange of mass between a WTD and the ambient fluid is large because of the unstable trajectory. An atmospheric blocking, however, remains quasi-stationary for long periods. Therefore mass exchange should be small according to the results of the point-vortex model. But the interpretation of an atmospheric blocking as a dipolar vortex has yet to overcome some difficulties, in the first place its surprising stability.

We thank two anonymous reviewers for their critical comments on an earlier version of this paper. O.U.V.F. gratefully acknowledges financial support from the Netherlands Foundation for Fundamental Research on Matter (FOM).

REFERENCES

CREMERS, B. E. & VELASCO FUENTES, O. U. 1994 Chaotic advection by dipolar vortices on a topographic β-plane. In *Modelling of Oceanic Vortices* (ed. G.J.F. van Heijst), Verhandelingen Koninklijke Nederlandse Akademie van Wetenschappen. North-Holland.

HOBSON, D. D. 1991*a* Point vortex models for modon dynamics. PhD thesis, California Institute of Technology.

HOBSON, D. D. 1991*b* A point vortex dipole model of an isolated modon. *Phys. Fluids* A 3, 3027–3033.

HORTON, W. 1984 Drift wave turbulence and anomalous transport. In *Handbook of Plasma Physics*, vol. 2. Elsevier.

KLOOSTERZIEL, R. C., CARNEVALE, G. F. & PHILIPPE, D. 1993 Propagation of barotropic dipoles over topography in a rotating tank. *Dyn. Atmos. Oceans* **19**, 65–100.

KONO, J. & YAMAGATA, T. 1977 The behaviour of a vortex pair on the beta plane. *Proc. Oceanogr. Soc. Japan* **36**, 83–84 (In Japanese).

MAKINO, M., KAMIMURA, T. & TANIUTI, T. 1981 Dynamics of two dimensional solitary vortices in a low-β plasma with convective motion. *J. Phys. Soc. Japan* **50**, 980–989.

MCWILLIAMS, J. C. 1980 An application of equivalent modons to atmospheric blocking. *Dyn. Atmos. Oceans* **5**, 43–66.

NYCANDER, J. & ISICHENKO, M. B. 1990 Motion of dipole vortices in a weakly inhomogeneous medium and related convective transport. *Phys. Fluids* B **2**, 2042–2047.

ROM-KEDAR, V., LEONARD, A. & WIGGINS, S. 1990 An analytical study of transport, mixing and chaos in an unsteady vortical flow. *J. Fluid Mech.* **214**, 347–394.

VELASCO FUENTES, O. U. 1994 Propagation and transport properties of dipolar vortices on a γ plane. *Phys. Fluids* **6**, 3341–3352.

VELASCO FUENTES, O. U. & HEIJST, G. J. F. VAN 1994 Experimental study of dipolar vortices on a topographic β-plane. *J. Fluid Mech.* **259**, 79–106 (referred to herein as VFvH).

WIGGINS, S. 1992 *Chaotic Transport in Dynamical Systems*. Springer.

YABUKI, K., UENO, K. & KONO, M. 1993 Propagations and collisions of drift wave vortices in a cylindrical plasma. *Phys. Fluids* B **5**, 2853–2857.

ZABUSKY, N. J. & MCWILLIAMS, J. C. 1982 A modulated point-vortex model for geostrophic, β-plane dynamics. *Phys. Fluids* **25**, 2175–2182.